Journal of Power Sources 232 (2013) 23–28

Contents lists available at SciVerse ScienceDirect

Journal of Power Sources

journal homepage: www.elsevier.com/locate/jpowsour

Mathematical model of the dendritic growth during lithium electrodeposition

Rohan Akolkar*

Department of Chemical Engineering, Case Western Reserve University, A. W. Smith Building, Room 127, 10900 Euclid Avenue, Cleveland, OH 44106, USA

HIGHLIGHTS

- ► Mathematical model of dendrite growth during lithium electrodeposition is presented.
- ► Overpotential analysis shows that dendrites grow purely under activation control.
- ► Model predictions are compared with experimental data on dendrite growth rates.
- ► Dendrite growth can occur, albeit slowly, well below the limiting current.
- ► Dendritic growth is suppressed in systems exhibiting a lower transfer coefficient.

ARTICLE INFO

Article history:
Received 26 July 2012
Received in revised form
16 December 2012
Accepted 3 January 2013
Available online 11 January 2013

Keywords:
Lithium
Electrodeposition
Dendrites
Modeling

ABSTRACT

Dendritic growth of lithium during galvanostatic electrodeposition is modeled. The time-dependent concentration distribution near the lithium surface is computed by numerically solving the transport equation inside the diffusion boundary layer. The dendrite propagation rate, i.e., the dendrite tip current density, is calculated by analyzing the various overpotentials that develop at the dendrite tip and at the flat electrode surface. The surface overpotential at the dendrite tip due to its radius of curvature is also incorporated in the model; however, for typical dendrite tip radii, it is shown that this surface overpotential is very small. The dendrite tip propagation rate predicted by the model agrees reasonably well with experimental data from the literature. For dendritic growth under pure activation control, a simplified analytical expression for the tip current density is derived. The analytical expression shows that dendritic growth is suppressed in systems that exhibit a lower charge transfer coefficient.

1. Introduction

High energy density lithium (Li) metal batteries [1,2] are of interest for several applications, including electric vehicles (EVs) and portable electronics. Unlike conventional Li-ion batteries, the negative electrode (anode) in Li metal batteries is pure lithium. Li is highly electronegative (−3.04 V vs. standard hydrogen electrode) and is the lightest metal (0.534 g cm^{-3}). These properties translate into a battery system with large open circuit potential and specific energy. However, efforts to commercialize rechargeable Li metal battery technology have largely been unsuccessful due to their poor cycleability. A major roadblock is the issue of surface morphology evolution and dendritic growth observed during Li electrodeposition–electrodissolution cycles [3]. While the detailed mechanistic understanding of the Li dendrite formation is lacking, it has been hypothesized that dendrites grow due to non-uniform current distribution on the Li surface. The non-uniform current distribution is the result of surface heterogeneities, either in the form of roughness elements or non-uniformities in the solid electrolyte interphase (SEI) layer that forms on a Li surface in organic electrolytes. During battery discharge (i.e., Li electrodissolution), Li dendrites can detach from the electrode surface leaving loose Li crystals. This “dead” lithium is a major source of battery energy density loss. Additionally, sharp Li dendrites can cause internal shorts leading to thermal runaway and battery explosion. Thus, understanding and stabilizing the dendritic growth during Li electrodeposition is central to developing secondary Li metal battery technology.

The phenomenon of dendritic growth during electrodeposition is common to many metal systems. Barton and Bockris [4] studied the growth of silver dendrites from a silver nitrate electrolyte and formulated a mathematical model for predicting the dendrite tip radius and the tip propagation rate. Diggle et al. [5] and Oren and

* Tel.: +1 216 368 4151.
E-mail address: rna3@case.edu.

0378-7753/$ – see front matter © 2013 Elsevier B.V. All rights reserved.
http://dx.doi.org/10.1016/j.jpowsour.2013.01.014

Landau [6] extended the Barton and Bockris model to the electrocrystallization of zinc. Recently, Pasquale et al. [7] reported the formation of dendritic copper electrodeposits from acidic electrolytes and the effect of additives on the dendrite morphology evolution. Formation of dendrites during lithium electrodeposition has also been studied by numerous investigators [8–14]. Crowther and West [8] and Nishikawa et al. [9] reported *in situ* observations of the effect of electrolyte composition (i.e., salt and solvent concentration) and current density on the lithium dendrite initiation time and the dendrite growth rate. In a similar experimental study of the dendrite initiation time, Park et al. [10] used frequency impedance and voltage transients to quantify the effect of temperature on lithium dendrite growth. Ishikawa et al. [11] reported the effect of electrolyte additives in suppressing the dendritic growth by favorably modifying the lithium surface film. Brissot et al. [12] observed the onset of dendrites in lithium/polymer cells at various current densities and correlated the dendrite initiation time to the Sand's time predicted by Chazalviel [13]. Recently, Monroe and Newman [14] presented a comprehensive mathematical model of the time evolution of dendrite tip height and growth velocity in Li/polymer cells.

Numerical models of lithium dendritic growth, such as the model presented by Monroe and Newman [14], are computationally complex. In the present work, a simplified approach is developed to analyze the various overpotentials underplay at the dendrite tip and at the flat electrode surface. Analysis of the overpotentials leads to a simplified expression for the dendrite tip current density in terms of the various system parameters, i.e., the operating current density, transport properties, and electrodeposition kinetics (represented by the cathodic transfer coefficient). It is shown that the dendrite tip current density, when translated into the dendrite growth rate, agrees reasonably well with experimental observations (from literature) of dendritic lithium electrodeposits.

2. Mathematical formulation

In this section, a mathematical model for the lithium dendritic growth is developed. The model consists of two parts: (i) An unsteady-state transport model that provides the Li^+ ion concentration in the vicinity of the electrode surface, and (ii) An electrochemical reaction model that couples the activation, concentration and surface curvature overpotentials to provide the dendrite tip current density.

2.1. Lithium ion transport model

A schematic representation of the model geometry is shown in Fig. 1. The model consists of a lithium surface in contact with a Li^+ containing liquid electrolyte. A diffusion layer of thickness δ is present in the vicinity of the electrode surface. It is assumed that a small hemispherical dendrite 'precursor' of radius r is present on the electrode surface. Since the dendrite precursor radius is small in comparison to the diffusion layer thickness, it does not appreciably affect the Li^+ concentration profile in the diffusion layer. To model ionic transport, the generalized convective diffusion equation given by Newman [15] for electrochemical systems is invoked. For a binary electrolyte (e.g., $LiPF_6$) without supporting electrolyte, material balance provides [15]:

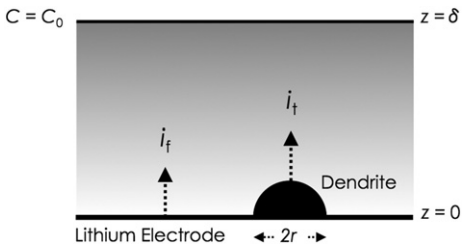

Fig. 1. Schematic representation of the model lithium surface used in this study. A hemispherical dendrite 'precursor' of radius r is present on the lithium surface. The dendrite tip grows at a current density i_t, and the flat electrode surface grows at a current density i_f.

$$\frac{\partial C}{\partial t} + \vec{v}\cdot\nabla C = \nabla\cdot(D\nabla C) - \frac{i\cdot\nabla t_+}{z_+ F} \quad [1]$$

Eq. (1) represents the generalized material balance equation that governs the time-dependent concentration (C) distribution. In Eq. (1), D is the diffusion coefficient, t_+ is the Li^+ transport number, z_+ is the charge number, i is the current density, and $\vec{v}$ is the fluid velocity. The first term on the right hand side of Eq. (1) represents transport by diffusion, and the second term on the right hand side represents ionic migration. Since convective transport inside the boundary layer can be assumed to be zero, Eq. (1) simplifies to:

$$\frac{\partial C}{\partial t} = \nabla\cdot(D\nabla C) - \frac{i\cdot\nabla t_+}{z_+ F} \quad [2]$$

In typical organic electrolytes used for lithium electrodeposition, the variation of the Li^+ transport number with salt concentration is negligible [16]. Equation (2) then reduces to the Fick's second law of diffusion:

$$\frac{\partial C}{\partial t} = \nabla\cdot(D\nabla C) \quad [3]$$

In its one-dimensional form, Eq. (3) can be written as:

$$\frac{\partial C}{\partial t} = \frac{\partial}{\partial z}\left(D\frac{\partial C}{\partial z}\right) \quad [4]$$

The above formulation of the transport model is analogous to prior approaches, e.g., by Monroe and Newman [14] and Nishikawa et al. [17]. However, in the present approach, a concentration-dependent diffusion coefficient is incorporated into the model. Following Stewart and Newman [18], the concentration dependence is expressed as:

$$D = ae^{-bC} \quad [5]$$

The constants $a = 2.582\times10^{-5}\ cm^2\ s^{-1}$ and $b = 2.856\ M^{-1}$ were determined experimentally [18]. The transport equation (Eq. (4)) then becomes:

$$\frac{\partial C}{\partial t} = \frac{\partial}{\partial z}\left(ae^{-bC}\frac{\partial C}{\partial z}\right) \quad [6]$$

In the absence of forced convection, as is the case in a lithium battery, the diffusion boundary layer thickness δ is determined primarily by natural convection. Ota et al. [19] reported *in situ* measurements of the diffusion layer thickness on a vertical lithium electrode using holographic interferometry. A diffusion layer thickness δ of about 400 μm was reported [19]. This diffusion layer thickness agrees well with that predicted using the empirical correlations of dimensionless groups for electrochemical mass transfer to a vertical electrode outlined by Ibl [15,20]. Thus, $\delta = 400$ μm was used in the analysis that follows. For the model geometry considered in the present study (Fig. 1), following initial and boundary conditions apply:

$$\text{At } t = 0: \quad C = C_0 \tag{7}$$

$$\text{At } z = \delta: \quad C = C_0 \tag{8}$$

$$\text{At } z = 0: \quad D\frac{dC}{dz} = \frac{i_f(1-t_+)}{nF} \tag{9}$$

In Eqs. (7) and (8), C_0 is the bulk concentration. Eq. (9) represents a galvanostatic boundary condition at the electrode surface where the current density is set to i_f. While i_f is defined as the current density on the flat portion of the Li surface, it can also be taken as the average operating current density (i_{avg}) on the entire electrode surface. This is true when the Li dendrite growth occurs only on a very small fraction of the electrode surface. When i_f is well below the limiting current density, the Li^+ concentration near the electrode is close to its bulk concentration (C_0). When i_f approaches the limiting current density, the Li^+ concentration close to the electrode surface approaches zero.

Equation (6) along with the initial and boundary conditions of Eqs. (7)–(9) constitute a transport model that can be solved numerically to determine the time-dependent concentration distribution within the boundary layer.

2.2. Electrochemical reaction model at the lithium surface

At a constant current density (i_f) applied to the flat lithium surface, the total overpotential (η_f) that develops at the flat surface is the sum of the activation overpotential ($\eta_{a,f}$) and the concentration overpotential ($\eta_{c,f}$). Assuming Tafel kinetics for the activation overpotential, the total overpotential at the flat electrode surface is:

$$\eta_f = \eta_{a,f} + \eta_{c,f} = \frac{RT}{\alpha_c F}\ln\left(\frac{i_f}{i_0}\right) - \frac{RT}{nF}\ln\left(\frac{C_e}{C_0}\right) \tag{10}$$

In Eq. (10), α_c is the cathodic transfer coefficient, i_0 is the exchange current density and C_e is the lithium concentration at the electrode surface provided by solution of Eq. (6). All overpotentials are assumed to be positive, thereby necessitating the use of a negative sign preceding the concentration overpotential term.

The total overpotential (η_t) at the tip of the dendrite precursor is the sum of the activation overpotential ($\eta_{a,t}$), concentration overpotential ($\eta_{c,t}$) and the overpotential due to the surface energy of the curved dendrite tip ($\eta_{s,t}$). The latter surface overpotential is directly proportional to the surface tension at the electrode–electrolyte interface (γ) and inversely proportional to the dendrite tip radius (r). Thus, the total overpotential at the dendrite tip is:

$$\eta_t = \eta_{a,t} + \eta_{c,t} + \eta_{s,t} = \frac{RT}{\alpha_c F}\ln\left(\frac{i_t}{i_0}\right) - \frac{RT}{nF}\ln\left(1 - \frac{i_t}{i_{L,t}}\right) + \frac{2\gamma K}{nFr} \tag{11}$$

In Eq. (11), K is the molar volume of lithium and $i_{L,t}$ represents the limiting current density at the dendrite tip. It should be noted that Li^+ diffusion to the dendrite tip is spherical, unlike linear diffusion to the flat electrode surface [5]. The limiting current density at the tip is thus:

$$i_{L,t} = \frac{nFDC_t}{(1-t_+)r} \tag{12}$$

In Eq. (12), C_t is the Li^+ concentration in the vicinity of the dendrite tip. Substituting Eq. (12) into Eq. (11):

$$\eta_t = \frac{RT}{\alpha_c F}\ln\left(\frac{i_t}{i_0}\right) - \frac{RT}{nF}\ln\left[1 - \frac{i_t(1-t_+)r}{nFDC_t}\right] + \frac{2\gamma K}{nFr} \tag{13}$$

Let us assume that the potential applied to the electrode surface is V (with respect to a Li/Li^+ reference). By definition:

$$V - \phi_f = \eta_f \tag{14}$$

$$V - \phi_t = \eta_t \tag{15}$$

where ϕ_f is the potential in solution near the flat surface, and ϕ_t is the potential in solution near the dendrite tip. Subtracting Eq. (15) from Eq. (14):

$$\eta_f - \eta_t = \phi_t - \phi_f = \Delta\phi \tag{16}$$

Thus, the difference in the net overpotential at the flat lithium surface and that at the dendrite tip is equal to the solution potential difference $\Delta\phi$ between the flat surface and the dendrite tip. $\Delta\phi$ can be estimated as $i_{avg}l_c/\kappa$ where the dendrite length can be taken as the characteristic length (l_c). For dendrites that are ~10 μm long (as shown below), and assuming i_{avg} = 10 mA cm^{-2} and κ = 10 mS cm^{-1}, we get $\Delta\phi \sim 1$ mV which is negligible in comparison to the net overpotentials. It is thus assumed that $\Delta\phi = 0$. This leads to the equipotential surface approximation:

$$\eta_f = \eta_t \tag{17}$$

Inserting the overpotential expressions from Eq. (10) and Eq. (13) into Eq. (17):

$$\frac{RT}{\alpha_c F}\ln\left(\frac{i_f}{i_0}\right) - \frac{RT}{nF}\ln\left(\frac{C_e}{C_0}\right) = \frac{RT}{\alpha_c F}\ln\left(\frac{i_t}{i_0}\right) - \frac{RT}{nF}\ln\left[1 - \frac{i_t(1-t_+)r}{nFDC_t}\right] + \frac{2\gamma K}{nFr} \tag{18}$$

For the dendrite precursor tip to grow more rapidly than the flat surface, it is essential that the concentration overpotential at the tip (second term on the right hand side of Eq. (18)) be negligibly small. Physically, this condition is met due to spherical Li^+ diffusion to a curved (typically $r = 10^{-4}$–10^{-5} cm) dendrite tip that releases the tip from mass transport limitations. This has been demonstrated in several metal electrodeposition systems, such as zinc and silver electrodeposition [4,5]. It should also be recognized that as the dendrite tip moves away from the flat surface into the boundary layer, it experiences a gradually increasing local Li^+ concentration (C_t) further diminishing the effect of the concentration overpotential. Neglecting $\eta_{c,t}$ and rearranging Eq. (18) provides:

$$\frac{RT}{\alpha_c F}\ln\left(\frac{i_t}{i_f}\right) + \frac{RT}{nF}\ln\left(\frac{C_e}{C_0}\right) + \frac{2\gamma K}{nFr} = 0 \tag{19}$$

Eq. (19) relates the tip current density i_t to the flat surface current density i_f. If the concentration (C_e) near the flat surface is known (i.e., from solution of the transport model Eq. (6)), then the tip current density can be calculated as a function of the tip radius (r). A list of system parameters required to solve Eq. (6) and Eq. (19) is provided in Table 1. While the present study analyzes a generic

Table 1
Parameter values used in the mathematical model.

Parameter	Value	Source
Transfer coefficient	α_c = 0.2–0.4	Crowther and West [8]
Exchange current density	i_0 = 0.2 mA cm^{-2}	Crowther and West [8]
Li^+ bulk concentration	$C_0 = 10^{-3}$ mol cm^{-3}	Selected
Boundary layer thickness	δ = 400 μm	Ota et al. [19]
Interfacial surface tension	$\gamma = 4 \times 10^{-5}$ J cm^{-2}	Yamaki et al. [22]
Transference number	t_+ = 0.2	Xu [3]

lithium metal/liquid electrolyte system, parameter values have been chosen to best fit literature data on the specific case of lithium electrodeposition from a 1.0 M $LiPF_6$ salt in 1:1 PC:DMC solvent system [8].

3. Results and discussion

Numerical solution of Eq. (6) at an operating current density (i_f) of 10 mA cm^{-2} yielded a concentration distribution shown in Fig. 2. The concentration at the lithium electrode surface drops gradually from the bulk concentration (C_0) to about 30% of the bulk concentration over a time period of ~2500 s with majority of the concentration drop occurring in the first 300 s. The concentration profile enables estimation of the tip current density (i_t) using Eq. (19). This was done for three different values of the operating current density i_f, i.e., $i_f = 0.99i_{L,f}$ and $i_f = 0.90i_{L,f}$ (near the limiting current), and $i_f = 0.40i_{L,f}$ (below the limiting current). The limiting current density ($i_{L,f}$) in the system was estimated to be about 25.7 mA cm^{-2}; thus, the concentration distribution shown in Fig. 2 represents the operating condition $i_f = 0.40i_{L,f}$ closely. For $i_f = 0.99i_{L,f}$ and $i_f = 0.90i_{L,f}$, the concentration distributions were also computed numerically (not shown). At each value of operating current density i_f, two dendrite tip radii (i.e., 10^{-4} and 10^{-5} cm) were selected for analysis. These radii represent typical dendrite tip sizes encountered in electrodeposition processes [4–6,8,14]. The tip current densities computed from Eq. (19) for the various cases considered are tabulated in Table 2. It is observed that the tip current density is very large (247 mA cm^{-2}) when operating close to the mass transport limit (i.e., 99% of $i_{L,f}$). When operating below the mass transport limit (i.e., 40% of $i_{L,f}$), the tip current density is considerably lower (15.9 mA cm^{-2}); however, it is still about 60% higher than the flat surface current density. This suggests that lithium dendrites can grow, albeit slowly, even at operating current densities well below the Li^+ limiting current density, as observed by Crowther and West [8], and Nishikawa et al. [21].

Knowing i_t, it is now possible to compute the dendrite length as a function of time (or charge passed) using Faraday's law:

$$h = \frac{M}{n\rho F}\int_0^t i_t dt \qquad [20]$$

Equation (20) allows direct comparison of the model predictions with experimental data on dendrite propagation. Nishikawa et al. [21] provide the most comprehensive characterization of the dendritic growth rate in lithium electrodeposition. Using *in situ* microscopy, these investigators studied dendrite propagation as a function of the total charge passed under various operating conditions of current density and choice of electrolyte. In a 1 M $LiPF_6$–PC electrolyte, dendrite growth rates of 0.01–0.06 μm s^{-1} were reported. The large spread in measured propagation rates, also seen in other studies [8,17], was attributed to the non-uniform current distribution on the electrode surface. Nevertheless, an upper bound and a lower bound on the dendrite length as a function of the charge passed (C cm^{-2}) can be extracted from the experimental work of Nishikawa et al. [21] for comparison with model predictions. As shown in Fig. 3, model prediction is in the range of experimental data. While it may appear that the model prediction falls closer to the lower bound on the dendrite length, this may simply be due to differences in the kinetic or transport properties (α_c, D or δ) assumed in the present model and those present in the actual experimental system of Nishikawa et al. [21]. Further well-controlled experimental studies with detailed characterization of system parameters combined with modeling investigations are needed to improve the correlation.

Table 2
Model predictions for the dendrite tip current density (i_t) under various operating conditions ($i_f/i_{L,f}$) and at two different tip radii (r). The limiting current density $i_{L,f}$ was calculated to be 25.7 mA cm^{-2}.

Operating condition $i_f/i_{L,f}$	Tip radius r (cm)	Tip current density i_t (mA cm^{-2})
0.40	10^{-5}	15.9
0.40	10^{-4}	16.1
0.90	10^{-5}	87.3
0.90	10^{-4}	88.6
0.99	10^{-5}	243
0.99	10^{-4}	247

3.1. Analytical model for the tip current density

The knowledge of the dendrite tip current density (i_t) as a function of the operating current density (i_f) allows for a comparative analysis of the various overpotentials underplay in lithium dendritic growth. The activation ($\eta_{a,f}$ and $\eta_{a,t}$), concentration ($\eta_{c,f}$) and surface curvature ($\eta_{s,t}$) overpotentials corresponding to the tip

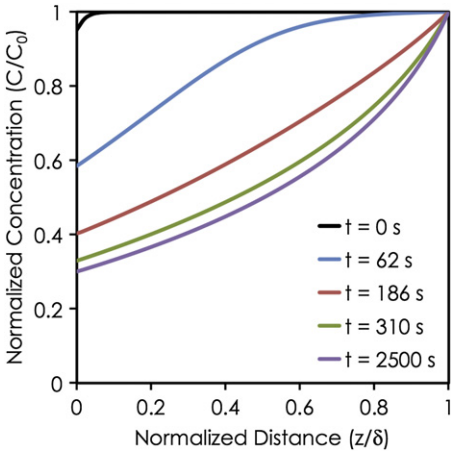

Fig. 2. Time evolution of the Li^+ concentration profiles within the boundary layer determined by numerical solution of the transport model (Eq. (6)). Galvanostatic lithium electrodeposition at a current density of 10 mA cm^{-2} is assumed.

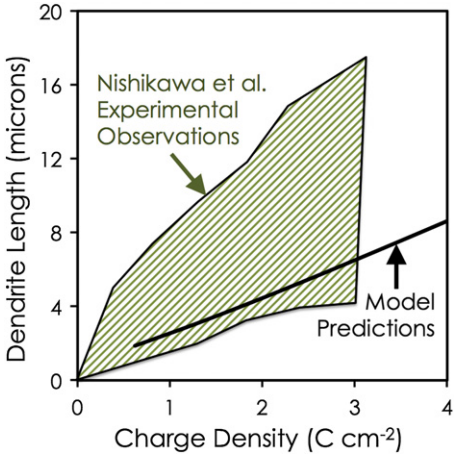

Fig. 3. Comparison of model prediction with experimental data on lithium dendrite propagation at an applied current density of 10 mA cm^{-2}. Experimental data is taken from the work of Nishikawa et al. [21]. The cross-hatched region represents the spread in the experimental data.

current density i_t and the flat surface current density i_f are plotted in Fig. 4. Fig. 4 shows overpotentials for the specific case of $i_f = 10$ mA cm^{-2}. It is observed that the three dominant overpotentials are the activation and concentration overpotentials at the flat electrode surface ($\eta_{a,f}$ and $\eta_{c,f}$) and the activation overpotential at the dendrite tip ($\eta_{a,t}$). In comparison to these overpotentials, the surface curvature overpotential ($\eta_{s,t}$) is at least an order of magnitude lower and thus negligible. For typical tip radius (10^{-4}–10^{-5} cm), the surface curvature overpotential ($\eta_{s,t} = 2\gamma K/nFr$) was estimated, using parameters from Table 1, to be about 1 mV, and negligibly small. The validity of the assumption to neglect $\eta_{s,t}$ was also confirmed at operating conditions closer to the limiting current. Eliminating $\eta_{s,t}$ from Eq. (19) and rearranging provides:

$$\frac{i_t}{i_f} = \left(\frac{C_e}{C_0}\right)^{-\frac{\alpha_c}{n}} \quad [21]$$

The ratio C_e/C_0 is time-dependent; however, when the system reaches steady-state, an analytical expression for C_e/C_0 is possible from the solution of Eq. (6). Under galvanostatic steady-state conditions, the solution is:

$$\frac{C_e}{C_0} = -\frac{1}{bC_0}\ln\left[e^{-bC_0} + \frac{i_f(1-t_+)b\delta}{nFa}\right] \quad [22]$$

From Eq. (22), it is recognized that the limiting current density ($i_{L,f}$) on the flat lithium surface is:

$$i_{L,f} = \frac{nFa\left(1-e^{-bC_0}\right)}{(1-t_+)b\delta} \quad [23]$$

Combining Eq. (22) and (23) with Eq. (21):

$$\frac{i_t}{i_f} = \left\{-\frac{1}{bC_0}\ln\left[e^{-bC_0} + \frac{i_f}{i_{L,f}}\left(1-e^{-bC_0}\right)\right]\right\}^{-\frac{\alpha_c}{n}} \quad [24]$$

In Eq. (24), the ratio i_t/i_f represents the ratio of the dendrite tip current density to the current density on the flat surface. A higher i_t/i_f ratio corresponds to faster dendrite propagation. From Eq. (24), it is observed that i_t/i_f depends on four physical factors: (i) the ratio of the flat current density to the flat limiting current density ($i_f/i_{L,f}$) indicative of the operating regime of the lithium electrodeposition process, i.e., at or below the limiting current, (ii) the cathodic transfer coefficient (α_c) representative of the lithium electrodeposition kinetics, (iii) the bulk lithium concentration (C_0) and (iv) the parameter b representing the concentration dependence of the diffusion coefficient. A plot of i_t/i_f vs. $i_f/i_{L,f}$ at various α_c is shown in Fig. 5. It is clearly seen that dendrite propagation rates are largest when operating close to the limiting current density ($i_f \rightarrow i_{L,f}$). However, even below the limiting current (e.g., $i_f/i_{L,f} = 0.4$), the i_t/i_f ratio is about 1.6 which corresponds to slow but steady overgrowth of the dendrite tip over the flat electrode surface. Table 3 summarizes the tip current density provided by the simplified analytical model (Eq. (24)) compared to the numerical model (Eq. (6) together with Eq. (19)). Good agreement is observed between the two models.

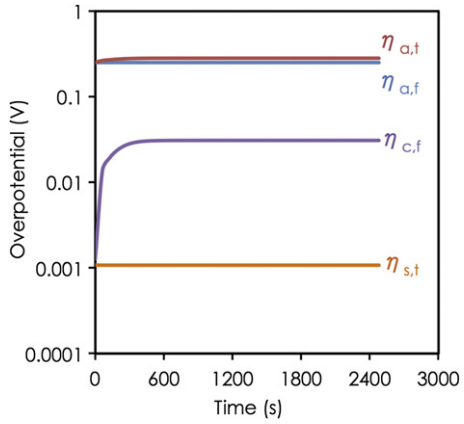

Fig. 4. Time evolution of the various overpotentials. The dominant overpotentials in the system are the activation overpotentials ($\eta_{a,f}$ and $\eta_{a,t}$) and the concentration overpotential at the flat electrode surface ($\eta_{c,f}$). The concentration overpotential at the dendrite tip ($\eta_{c,t}$, not shown) and the surface curvature overpotential ($\eta_{s,t}$) are negligible. Assumptions: $i_f = 10$ mA cm^{-2} and $r = 10^{-5}$ cm.

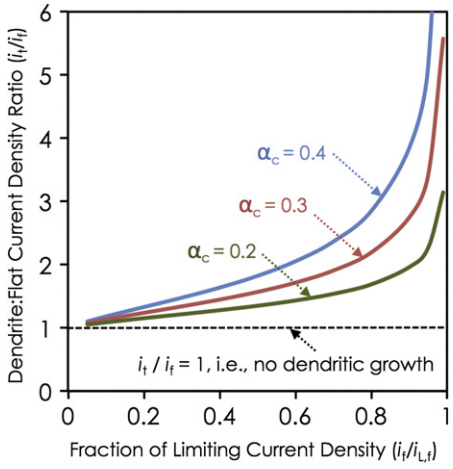

Fig. 5. The ratio of dendrite tip current density (i_t) to the flat surface current density (i_f) is a measure of the dendrite propagation rate. Fast dendritic growth is favored when operating near the limiting current ($i_f/i_{L,f}$ close to unity); however, slow but sustained dendritic growth can occur well below the limiting current density. Dendrite growth is suppressed in systems that exhibit a lower cathodic transfer coefficient.

The analytical model presented above provides valuable insights into the role of electrode kinetics in suppressing the lithium dendrite growth. Fig. 5 demonstrates that the ratio of dendrite: flat surface current density is lowered in systems that exhibit lower cathodic transfer coefficient α_c. This effect is pronounced when operating close to the limiting current, but diminishes gradually as the operating current density is lowered. The role of the cathodic transfer coefficient in modulating the lithium dendrite growth agrees well with the experimental findings of Crowther and West [8], who showed that dendrite formation is slower in electrolytes containing 1.0 M $LiPF_6$ + DMC solvent (which exhibit a lower α_c) than in electrolytes containing 1.0 M $LiPF_6$ + PC solvent (which exhibit a higher α_c). The role of the solvent in modifying the deposition kinetics is believed to be via the modification of the solid electrolyte interphase (SEI) layer on the lithium surface [23]. Further studies on the mechanistic role of the SEI layer in modifying the deposition kinetics are needed to establish a more fundamental understanding of the dendritic growth mechanisms in lithium electrodeposition [24].

Table 3
Comparison of numerical (Eqns. (6) and (19)) and analytical (Eq. (24)) models.

$i_f/i_{L,f}$	i_t/i_f from numerical model	i_t/i_f from analytical model
0.40	1.61	1.62
0.90	3.83	3.84
0.99	9.71	9.83

4. Conclusions

A mathematical model of the dendritic growth process during lithium electrodeposition is developed. The model incorporates transient diffusional transport of lithium ions in the diffusion boundary layer near the lithium surface along with electrochemical reactions (deposition) at the flat surface and at the dendrite tip. A concentration-dependent diffusion coefficient is incorporated in the transport model. The activation, concentration and surface energy overpotentials at a dendrite 'precursor' tip are compared to the activation and concentration overpotentials on the flat electrode surface. Analysis of the overpotentials leads to a simplified analytical expression (Eq. (24)) for the dendrite tip current density (i_t) in terms of systems parameters such as the operating current density on the flat electrode surface (i_f) and the cathodic transfer coefficient (α_c). Following key conclusions can be drawn:

(i) Dendritic growth during lithium electrodeposition can occur even when operating well below the limiting current density. However, in this case, dendrite growth rates are relatively slow. The numerical diffusion-reaction model proposed herein estimates dendrite growth rates of about 0.02 μm s^{-1} at an operating current density of 10 mA cm^{-2} comparable with experimentally observed [21] dendrite propagation rates.

(ii) A simplified analytical expression for the dendrite tip current density is derived when the concentration and surface curvature overpotentials at the dendrite tip are negligible, i.e., dendritic growth is under pure activation control. The simplified analytical model predictions agree well with the more comprehensive numerical model.

(iii) Dendritic growth can be slowed, but not completely suppressed, by lowering the cathodic transfer coefficient, which has the effect of increasing the activation resistance and 'leveling' the surface morphology evolution during electrodeposition.

References

[1] B. Scrosati, J. Garche, J. Power Sources 195 (2010) 2419–2430.
[2] P. Andrei, J. Zheng, M. Hendrickson, E. Plitchta, J. Electrochem. Soc. 159 (6) (2012) A770–A780.
[3] K. Xu, Chem. Rev. 104 (2004) 4303–4417.
[4] J. Barton, J. Bockris, Proc. Roy. Soc. (London) A268 (1962) 485–505.
[5] J. Diggle, A. Despic, J. Bockris, J. Electrochem. Soc. 116 (11) (1969) 1503–1514.
[6] Y. Oren, U. Landau, Electrochim. Acta 27 (6) (1982) 739–748.
[7] M. Pasquale, D. Barkey, A. Arvia, J. Electrochem. Soc. 152 (3) (2005) C149–C157.
[8] O. Crowther, A. West, J. Electrochem. Soc. 155 (11) (2008) A806–A811.
[9] K. Nishikawa, T. Mori, T. Nishida, Y. Fukunaka, M. Rosso, T. Homma, J. Electrochem. Soc. 157 (11) (2010) A1212–A1217.
[10] H. Park, C. Hong, W. Yoon, J. Power Sources 178 (2008) 765–768.
[11] M. Ishikawa, S. Machino, M. Morita, J. Electroanal. Chem. 473 (1999) 279–284.
[12] C. Brissot, M. Rosso, J. Chazalviel, S. Lascaud, J. Power Sources 81–82 (1999) 925–929.
[13] J. Chazalviel, Phys. Rev. A 42 (1990) 7355.
[14] C. Monroe, J. Newman, J. Electrochem. Soc. 150 (10) (2003) A1377–A1384.
[15] J. Newman, Electrochemical Systems, Prentice-Hall, Englewood Cliffs, NJ, 1991.
[16] L. Ole Valøen, J.N. Reimers, J. Electrochem. Soc. 152 (5) (2005) A882–A891.
[17] K. Nishikawa, Y. Fukunaka, T. Sakka, Y.H. Ogata, J.R. Selman, J. Electrochem. Soc. 154 (10) (2007) A943–A948.
[18] S. Stewart, J. Newman, J. Electrochem. Soc. 155 (2008) F13–F16.
[19] M. Ota, S. Izuo, K. Nishikawa, Y. Fukunaka, E. Kusaka, R. Ishii, J.R. Selman, J. Electroanal. Chem. 559 (2003) 175–183.
[20] N. Ibl, Electrochim. Acta 1 (1959) 117–129.
[21] K. Nishikawa, T. Mori, T. Nishida, Y. Fukunaka, M. Rosso, J. Electroanal. Chem. 661 (2011) 84–89.
[22] J. Yamaki, S. Tobishima, K. Hayashi, K. Saito, Y. Nemoto, M. Arakawa, J. Power Sources 74 (1998) 219–227.
[23] E. Peled, J. Electrochem. Soc. 126 (1979) 2047.
[24] M. Mori, Y. Naruoka, K. Naoi, D. Fauteux, J. Electrochem. Soc. 145 (7) (1998) 2340–2348.